ELSEVIER

Thin Solid Films 398–399 (2001) 391–396

thin Solid films

www.elsevier.com/locate/tsf

Microstructure and mechanical properties of nanocomposite (Ti,Si,Al)N coatings

S. Carvalho[a,*], L. Rebouta[a], A. Cavaleiro[b], L.A. Rocha[c], J. Gomes[c], E. Alves[d]

[a]*Departamento de Física, Universidade do Minho, Campus de Azurém, 4800-058, Guimarães, Portugal*
[b]*ICMES — Faculdade de Ciências e Tecnologia da Universidade de Coimbra, 3030 Coimbra, Portugal*
[c]*Departamento de Mecânica, Universidade do Minho, Campus de Azurém, 4800-058, Guimarães, Portugal*
[d]*ITN, Departamento de Física, E.N. 10, 2686-953 Sacavém, Portugal*

Abstract

In this work (Ti,Si,Al)N films were deposited using only rf or a combination of rf and d.c. reactive magnetron sputtering. Chemical composition, thickness, film structure and mechanical properties of the films were investigated by means of Rutherford backscattering (RBS), electron microprobe analysis (EPMA), ball-cratering, X-ray diffraction (XRD) and ultramicroindentation, respectively. All samples showed high hardness values, exceeding, in some cases, 50 GPa. XRD results revealed the formation of a mixture of two phases whose structure is similar to TiN. One phase is noted as being TiN bulk with a lattice parameter of 0.428 nm and develops only in conditions of high surface mobility. This behaviour can be associated with the segregation of the SiN_x phase, though the formation of an amorphous AlN phase cannot be excluded. Another phase, which is noted as Ti–Si–Al–N ($a \approx 0.420$ nm), where Si and Al atoms substitute the Ti atoms on the TiN lattice, develops in situations of lower surface mobility. The thermal stability of these coatings was studied by thermal treatments in a vacuum atmosphere, where it was found that a small increase in hardness was obtained after 1 h heat treatment at 800°C.

Keywords: Nanocomposites; Superhard coatings; Ti–Si–Al–N; Microstructure; Thermal stability; Wear coefficient

1. Introduction

TiN single layer coatings, as the traditional hard coatings, played an important role in the early development stage to improve the wear resistance of cutting and forming tools. One of the drawbacks of TiN is its limited oxidation resistance at high temperatures that can be reached during cut process. Although TiN shows good wear resistance, new materials with significantly improved properties concerning wear and oxidation resistance are being used to replace TiN in numerous applications [1]. These materials are of a more complicated structure, as there are ternary and quaternary systems [2]. (Ti,Al)N coatings exhibit a great improvement in oxidation resistance when compared with TiN coatings and can be used at temperatures up to 800°C [3–6]. Aluminium forms a stable oxide layer at the surface of these films upon exposure to oxidizing conditions, thus protecting the underlying (Ti,Al)N [7]. Important criteria for the suitability of a material for tribological applications concern not only resistance against oxidation, but also high hardness, stiffness and a low friction coefficient. Therefore, nanocomposite coatings materials have recently attracted increasing interest due to the possibility of combining all these properties. The most studied system up to now, and which revealed the most promising results, is the (Ti,Si)N system [8–12]. These films were characterised as being nanocomposites consisting of TiN cubic nanocrystallites embedded in an amorphous matrix of silicon nitride (nc-TiN/a-Si_3N_4) and were prepared by plasma chemical vapour (PCVD), reaching a Vickers microhardness in the range of 80–105 GPa [13]. The superhardness of these composites depends on the crystalline

* Corresponding author. Tel.: +351-253-510154; fax: +351-253-510153.
E-mail address: nocas@fisica.uminho.pt (S. Carvalho).

0040-6090/01/$ - see front matter
PII: S0040-6090(01)01348-7

Table 1
Deposition parameters

Substrate temperature	200–500°C
Substrate rotation frequency	4 rev./min
Target to substrate distance	60 mm
d.c. Bias voltage	−100 to −25 V
Working pressure	5×10^{-1} Pa
Base pressure	2×10^{-4} Pa
Argon flow rate	100 sccm
rf or d.c. power (for Ti)	3.1–4.0 W/cm^2 or 6.4 mA/cm^2
rf power (for Si)	1.3–3.1 W/cm^2
d.c. Power (for Al)	1.5–2.6 mA/cm^2

and amorphous phases that all together must form strong materials with high cohesive energy at their interfaces. The usual mechanisms of deformation and mechanical failure are absent or hindered in such a material. Dislocations and other structural defects that may be formed during the deposition will become annihilated within the grain boundaries, so that even if formed under a high applied stress, the dislocations within the nanocrystals cannot glide through the amorphous grain boundary matrix [13]. This paper reports the results of the investigation of a quartenary nitride system — (Ti,Si,Al)N, and tries to understand the relationship between the mechanical properties (hardness, Young's modulus, elastic recovery) and the microstructure (nanocrystalline with individual phases). Particularly important are the applications that require high temperature operation; hence, special attention will be given to the temperature effects on microstructural changes in vacuum, and its correlation with the improvement of the mechanical properties.

2. Experimental

(Ti,Si,Al)N coatings were deposited onto refractory steel (AISI 310), high-speed steel (M2) and silicon substrates by rf or a combination of rf and dc power supply reactive magnetron sputtering in an Alcatel SCM 650 system. The depositions were carried out in an Ar+N_2 atmosphere and before each deposition the substrates were sputter-etched for 10 min in an Ar atmosphere with a 200 W rf power. Two series of samples were produced in rotation mode, from high-purity Ti, Si and Al targets. Some samples were prepared with the titanium target coupled to a rf source, while others were deposited using a d.c. power supply. A Ti adhesion layer of approximately 0.35 μm was deposited onto these samples before coating deposition. A third series of samples was produced in static mode with some pieces of Si and Al distributed symmetrically on the erosion zone of the Ti target, which was coupled to a rf power supply. Further detailed information regarding some deposition parameters is presented in Table 1.

The atomic composition of the as-deposited samples was determined by electron microprobe analysis (EMPA) and Rutherford backscattering (RBS). In order to extract the areal density, a proton beam of 1.6 MeV and a He^+ beam of 2 MeV were used in the RBS measurements. An average number of five 'ball cratering' (BC) experiments were performed in each sample in order to determine its thickness. Texture and structure were determined with X-ray diffraction (XRD) experiments using CuKα radiation. To evaluate the tribological properties, such as the wear and friction coefficient, pin-on-disk wear tests were carried out. After wearing with a Si_3N_4 pin at a 5 N normal load and at a speed of 0.5 ms^{-1} the disk wear track was checked with a profilometer. A computer-controlled Fischerscope H100 ultramicrohardness tester equipped with a Vickers diamond indenter was used in order to obtain the hardness values. A series of hardness measurements with maximum load values between 20 and 80 mN were performed with a sample with a hardness value of 48 GPa. For a maximum load of 40 mN, the hardness values were considered independent of the maximum load applied, and the indentation depths did not exceed one tenth of the coating thickness [14,15]. However, when the sample thickness and high hardness allowed the use of higher maximum loads, a value of 60 mN was used. A description of the necessary offset and thermal drift corrections can be found elsewhere [16–18]. On average, 10 tests were performed on each sample. For the vacuum annealing, the samples were introduced in a vertical furnace, then being subjected to a thermal cycle consisting of a heating time of 1.5 h up to the annealing temperature, 1 h being held at that temperature (600°C, 800°C, 900°C, 1000°C), followed by slow cooling to room temperature. All samples were analysed by XRD and indentation after heat treatment in vacuum in order to study the thermal stability of the microstructure and hardness.

3. Results and discussion

3.1. Chemical and structural analysis

Table 2 presents some experimental details as well as some results such as composition, thickness, density, hardness and the Young's modulus of typical (Ti,Si,Al)N samples.

Regarding the microstructure of the as deposited samples, two distinct phases were observed. An example of this behaviour is shown in Fig. 1 which represents the X-ray diffraction patterns obtained from samples 1, 2, 3 and 4. The first three samples (Fig. 1a–c) were prepared in static mode applying a power of 1000, 600 and 850 W, respectively, while the fourth sample (Fig. 1d) was deposited by rotation mode. The first sample is characterized by a strong narrow peak (FWHM≈0.3°) and three other weak peaks that match a cubic phase with a lattice parameter of 0.420 nm, similar to what

Table 2
Experimental details and some results of typical (Ti,Si,Al)N coatings

Sample	Composition	Ti (at.%)	Si (at.%)	Al (at.%)	Temp. (°C)	Bias voltage (V)
1	$Ti_{0.56}Si_{0.26}Al_{0.18}N$	28	13	9	300	−50
2	$Ti_{0.62}Si_{0.20}Al_{0.18}N$	31	10	9	300	−50
3	$Ti_{0.69}Si_{0.16}Al_{0.17}N_{0.98}$	34.5	8	8.5	300	−50
4	$Ti_{0.74}Si_{0.04}Al_{0.18}N_{0.98}$	39	4.5	6.5	300	−50
5	$Ti_{0.55}Si_{0.12}Al_{0.33}N$	27.5	6	16.5	300	−50
6	$Ti_{0.45}Si_{0.23}Al_{0.31}N$	22.5	11.5	15.5	300	−50
7	$Ti_{0.78}Si_{0.04}Al_{0.18}N$	39	2	9	400	−50
8	$Ti_{0.69}Si_{0.15}Al_{0.16}N$	34.5	7.5	8	400	−70
9	$Ti_{0.66}Si_{0.13}Al_{0.21}N$	33	6.5	10.5	400	−100
10	$Ti_{0.64}Si_{0.14}Al_{0.22}N$	32	7	11	400	−50

Sample	Mode	Power/Current Ti-Target	Thickness (μm)	Density (g/cm^3)	Hardness (GPa)	Young's Modulus (GPa)
1	static	1000 W	3.3	4.3	36	332
2	static	600 W	2.2	4.4	54	310
3	static	850 W	1.8	–	52	472
4	rotation	750 W	1.3	4.0	38	382
5	rotation	750 W	1.7	–	43	382
6	rotation	700 W	1.6	3.6	44	379
7	rotation	900 W	1.6	3.6	54	452
8	rotation	900 W	1.9	4.1	52	468
9	rotation	1.6 A	1.8	4.5	52	516
10	rotation	1.6 A	1.9	4.2	30	372

was obtained with the (Ti,Si)N samples [10] which revealed an fcc structure upon TEM observations [10,19], with grain sizes (>30 nm) and Si content (≈10 at.%) that justified the assumption that the Si atoms were substituting Ti atoms [10,19]. In this case, the Si atoms have six-fold coordination that is not usual for covalently bonded Si, but it was already found in other compounds [20,21]. The second sample (Fig. 1b) is characterized by a very broad peak (FWHM≈1.6°) that is usually associated with a smaller grain size. The indicated peaks match with a cubic phase that can be assigned to a NaCl type structure with a lattice parameter of 0.428 nm. This value is higher than the corresponding value of TiN bulk (0.424 nm), but justified by the residual stress effect on the peak positions (≈1%) [22,23]. An enhancement in mobility in the growing film and changes in ion-to-atom flux ratios are sufficient for the TiN phase to develop. With a change in rf power from 600 W to 1000 W, the deposition rate increased by a factor of almost 2, but the density bias current at the substrate only increased by a factor of approximately 1.2. This implies a decrease in the ion-to-atom flux ratio, and consequently, in the adatom surface mobility. An increase in the superficial mobility is enough to ensure the segregation of the Si atoms and consequent formation of an amorphous phase (SiN_x) and TiN nanocrystals. This behaviour is typical of Me_nN/SiN_x systems with transition metals, which form stable and strong nitrides, such as Ti, Zr, Hf, W [24–26]. If the formation of SiN_x as an amorphous phase is highly probable, the possible formation of an AlN amorphous phase cannot be excluded. The development of a-SiN_x and/or a-AlN phase covering the growth surface of the film grains limits the TiN crystal growth. The grain size of the film material decreases with increasing concentration of amorphous tissue material and can be as low as 1–10 nm [11,24,27]. The samples prepared with 850 W (static mode) and 750 W (rotation mode), associated with intermediate levels of adatom surface mobility, revealed little differences in its behaviour. Some samples exhibit an asymmetric broad peak where both phases are not markedly distinguished (Fig. 1c), corresponding to the peak centroid of an intermediate lattice parameter. This behaviour evidences a solid solution of both phases. Other samples with lower Si content clearly exhibit both phases (Fig. 1d). This can be explained by the alternating deposition of Ti and Si, although with a deposition rate of approximately 1 nm per rotation in order to avoid a multilayer structure. Furthermore, the low Si content also allows the definition of both phases.

3.2. Mechanical properties analysis

A superhard nanocomposite coating is characterized not only by its hardness, but also by its Young's modulus (E) and elastic recovery (W_e). The differences between

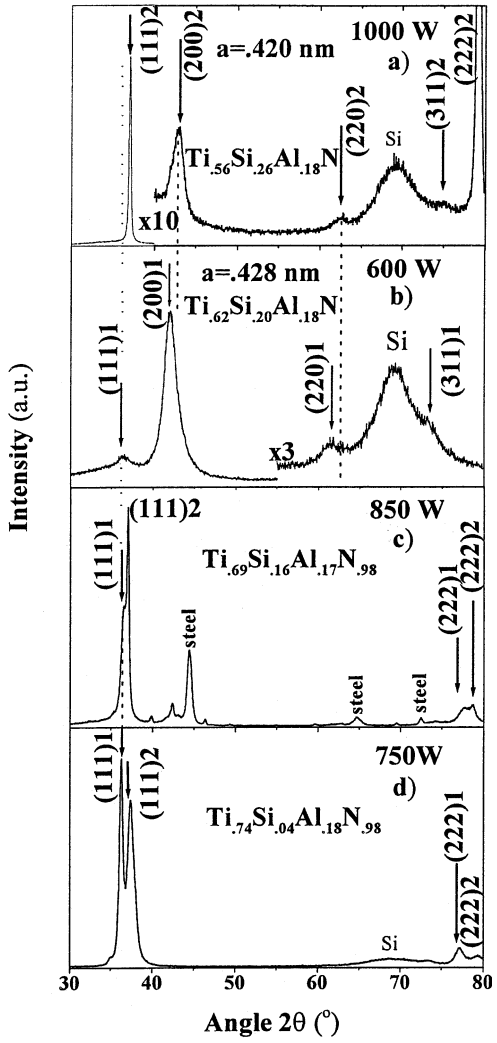

Fig. 1. X-Ray diffraction patterns of (Ti,Si,Al)N films deposited at same substrate temperature (300°C) and bias voltage (−50 V) on silicon and steel substrates.

hard and superhard (Ti,Si,Al)N coatings are not only evident on the microstructure and its hardness. The mechanical behaviour is also significantly different, as can be seen in Fig. 2 from the typical loading/unloading curves of ultramicroindentation measurements made on two (Ti,Si,Al)N samples. The hard sample exhibits a higher plastic deformation since the area between the loading and unloading curves is larger than for the superhard ones, having the latter a hardness of approximately 54 GPa and a high elastic recovery (74%). In contrast, the hard film, with a hardness of 30 GPa, exhibits a lower elastic recovery (24%). The correlation between high hardness and high elasticity is supported by the predicted behaviour of the nanocomposites under a high applied stress: due to the absence of dislocations no plastic deformation can occur. Instead, the formation of nanocracks (which cannot propagate) leads to a permanent brittle microfracture upon indentation. Because such nanocracks can easily close when the applied load is removed, a large elastic energy can be reversibly adsorbed by the material, leading to a kind of 'work hardening' [8].

Regarding the relationship between the hardness and the microstructure, it was found that the hardness of (Ti,Si,Al)N films is lower than 40 GPa (sample 1–36 GPa, sample 10–30 GPa) when the Ti–Si–Al–N phase is formed with a relatively large grain size, which is also evident from the peak width in diffraction patterns (Fig. 1a). This relatively high hardness is mainly due to the solution hardening.

An increase in hardness can be achieved when films are composed of smaller TiN grains — broad X-ray reflections (Fig. 1b) with a preferential (200) orientation. This preferential grain growth should be favourable to the increase on hardness since the crystals being oriented in the same direction (have low angle boundaries) should provide coherent interaction across the amorphous tissue [28,29]. This behaviour is in accordance with the Ti–Al–N system [28]. Additionally, the samples that are formed by the two described phases also show high hardness values (>50 GPa), which can be justified by the mixture of two hard phases as well as by the relatively low grain size.

Concerning the wear behaviour, the measurements that have been done did not yield a correlation between the hardness and the wear coefficient (see Table 3). Nevertheless, further experiments should be performed in order to acknowledge the tribological behaviour of these coatings.

3.3. Thermal stability

The superhardness of the nanocomposites is a simple consequence of the mechanical stability of its nanostructure. Therefore, the thermal stability of the nanos-

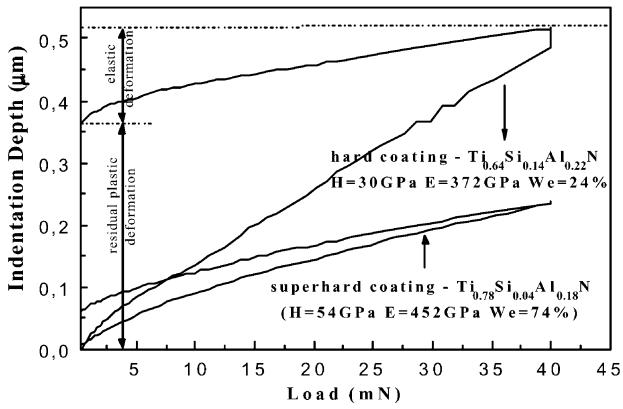

Fig. 2. Loading–unloading curve measured by a ultramicrohardness tester for a hard and a superhard (Ti,Si,Al)N coating. For each sample it is indicated the hardness (H), Young's modulus (E) and elastic recovery (W_e).

Table 3
Grain size, residual stress, recrystalization temperature

Sample	Composition	Grain size[a] (nm)	Residual stress[b] (GPa)	Recrystalization temperature (°C)	Wear coefficient $K\times10^{-14}$ (m^3/mN)	Friction coefficient μ
7	$Ti_{0.78}Si_{0.04}Al_{0.18}N$	<10	-6.0	≥900	8.4	0.78
8	$Ti_{0.69}Si_{0.15}Al_{0.16}N$	–	–	≥900	1.3	0.69
9	$Ti_{0.66}Si_{0.13}Al_{0.21}N$	–	-4.7	800	9.9	1.04
10	$Ti_{0.64}Si_{0.14}Al_{0.23}N$	>30	-3.8	800	–	–

[a] The grain size was estimated from the integral width of the Bragg peaks.
[b] The residual stress was calculated using Stoney's equation after measuring the parabolic deflections of the substrate (before and after deposition) by laser triangulation.

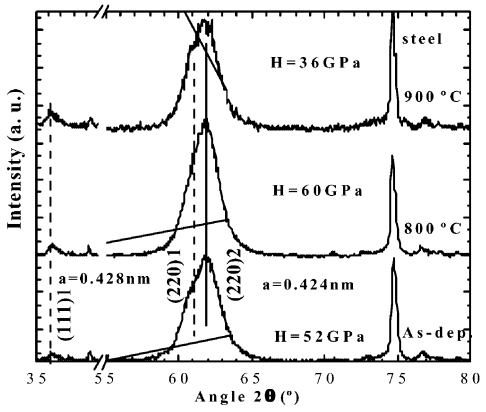

Fig. 3. XRD pattern evolution for $Ti_{0.69}Si_{0.15}Al_{0.16}N$ as a function of vacuum annealing temperature.

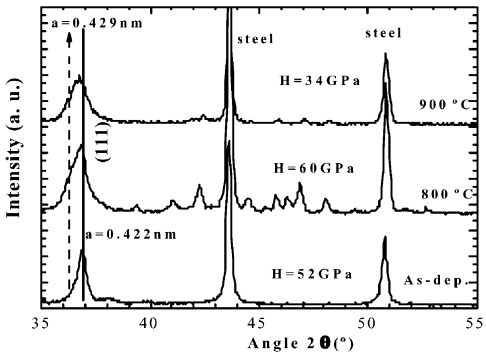

Fig. 4. XRD pattern evolution for $Ti_{0.66}Si_{0.13}Al_{0.21}N$ as a function of vacuum annealing temperature.

tructure should be the key for the stability of hardness, being crucial for industrial applications. Depending on their structure, the (Ti,Si,Al)N films revealed different behaviours during 1 h annealing in vacuum. Figs. 3 and 4 show the structural evolution of samples 8 and 9 in the initial state and after annealing at different temperatures in vacuum. In the first case, annealing at temperatures until 900°C, a significant change in the phase composition when compared with the initial phase was not encountered. However, on sample 9 (whose structure could be identified as a mixture of hard phases but with

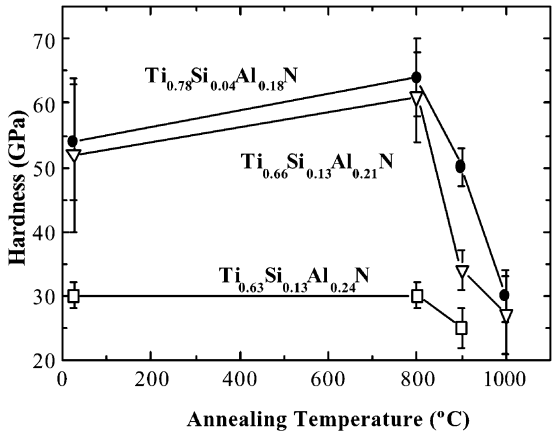

Fig. 5. Hardness values for as-deposited (Ti,Si,Al)N films and after annealing with 1 h in vacuum at indicated temperatures.

an intermediate lattice parameter), upon annealing at temperatures up to 800°C, a few changes in the phase composition compared with its initial state were observed. More precisely, a small peak shift towards lower 2θ angle values coupled with peak broadening was noted. After the annealing at 800°C. The formation of a TiN phase ($a=0.429$ nm) was observed. The increase in mobility promoted by the temperature rise stimulated the segregation of Si or Al atoms at the grain boundaries and the subsequent substitution of these atoms by Ti atoms in the fcc lattice [30,31]. However, from the peak position itself, the level of structural changes is not clearly understood.

The recrystallization temperature of the coatings that is estimated when a structural change is observed in the XRD patterns is presented in Table 3 as a function of the initial grain size, residual stress, and chemical composition.

Sample 7 was found to have the highest thermal stability, despite having a Si content of only 2 at.%. This observed high stability must be related to some kind of inherent thermodynamic stability, as such an energy reduction is a result of atomic rearrangements in the grain boundaries [32]. The inhibition of grain growth by strong segregation causes a reduction of the grain boundary specific energy, which results in a metastable

state that needs a high 'activation energy' for coarsening [13].

Fig. 5 displays the evolution of the hardness values with the annealing temperature. The hardest samples (7 and 9) increase their hardness values after annealing at 800°C, followed by a decrease at 900°C. A strong and stable interface is believed to be the origin of this stability, which also avoids the grain boundary sliding.

4. Conclusions

The present work demonstrates that nanostructured thin films within the (Ti,Si,Al)N system can be prepared by reactive magnetron sputtering. Furthermore, it was shown that for this system:

1. The formation of a mixture of two phases, whose structure is similar to TiN occurs. One phase is noted as TiN bulk with a lattice parameter of 0.428 nm and develops only in conditions of high surface mobility. This behaviour can be associated with the segregation of SiN_x phase; however, the formation of an amorphous AlN phase cannot be excluded. Another phase, which is noted as Ti–Si–Al–N, where Si and Al atoms substitute the Ti atoms in the TiN lattice, develops in situations of low surface mobility.
2. The superhardness correlates with a high elastic recovery. The hardest sample ($H=54$ GPa) exhibits a high elastic recovery (74%).
3. The sample whose structure is identified as a Ti–Si–Al–N solid solution presented hardness values close to 40 GPa. An increase in hardness was observed upon the formation of the nanocrystalline/amorphous phase.
4. For applications where the temperature of the coatings does not exceed 800°C, the (Ti,Si,Al)N system seems to be stable. In contrast, for applications where a temperature of 800°C or more is reached, it is necessary to have a higher control on the deposition parameters in order to obtain a specific structure.

Acknowledgements

The authors gratefully acknowledge the financial support from the FCT institution by the project no. POCTI/32670/CTM/2000, co-financed by European Community fund FEDER.

References

[1] F. Vaz, L. Rebouta, M.F. Da Silva, J.C. Soares, in: Y. Pauleau, P. Barna (Eds.), Protective Coatings and Thin Films: Synthesis, Characterization and Applications, Kluwer Acad. Publ, Dordrecht, 1996, p. 501.
[2] A. Niederhofer, P. Nesládek, H.-D. Männling, K. Moto, S. Veprek, M. Jílek, Surf. Coat. Technol. 120–121 (1999) 173.
[3] W.-D. Münz, J. Vac. Sci. Technol. A 4 (6) (1986) 2717.
[4] D. McIntyre, J.E. Greene, G. Hakansson, J.E. Sundgren, W.D. Munz, J. Appl. Phys. 67 (1990) 1542.
[5] S. Hofmann, H.A. Jehn, Surf. Interf. Anal. 12 (1988) 329.
[6] H.A. Jehn, S. Hofmann, W.-D. Münz, Thin Solid Films 153 (1987) 45.
[7] O. Knotek, M. Böhmer, T. Leyendecker, J. Vac. Sci. Technol. A 4 (1986) 2695.
[8] S. Veprek, Surf. Coat. Technol. 97 (1997) 15.
[9] X. Sun, J.S. Reid, E. Kolawa, M.-A. Nicolet, J. Appl. Phys. 81 (1997) 656.
[10] F. Vaz, L. Rebouta, B. Almeida, P. Goudeau, J. Pacaud, J.P. Rivière, J. Bessa Sousa, Surf. Coat. Technol 120–121 (1999) 166.
[11] S. Veprek, M. Haussmann, S.S. Reiprich, J. Vac. Sci. Technol., A 14 (1996) 46.
[12] M. Diserens, J. Patscheider, F. Lévy, Surf. Coat. Technol. 120–121 (1999) 158.
[13] S. Veprek, A. Niederhofer, K. Moto, T. Bolom, H.-D. Männling, P. Nesladek, G. Dollinger, A. Bergmaier, Surf. Coat. Technol. 133–134 (2000) 152.
[14] M.F. Doerner, D.S. Gardner, W.D. Nix, J. Mater. Res. 1 (1987) 845.
[15] C. Friedrich, G. Berg, E. Broszeit, C. Berger, Thin Solid Films 290–291 (1996) 216.
[16] A. Trindade, A. Cavaleiro, J. Fernandes, J. Test. Eval. 22 (1994) 365.
[17] J.M. Antunes, A. Cavaleiro, L.F. Menezes, M.I. Simões, J.V. Fernandes, Int. J. Mech. Sci. (2001), in press.
[18] F. Vaz, L. Rebouta, S. Ramos, M.F. da Silva, J.C. Soares, Surf. Coat. Technol. 108–109 (1998) 236.
[19] F. Vaz, L. Rebouta, Mater. Sci. Forum (2001) in press.
[20] A.-R. Grimmer, F. Von Lampe, M. Mägi, Chem. Phys. Lett. 132 (1986) 549.
[21] S. Muthupari, M.E. Fleet, J. Non-Crystal. Solids 238 (1998) 259.
[22] F. Vaz, L. Rebouta, R. Silva, M.F. Da Silva, J.C. Soares, Vacuum 52 (1999) 209.
[23] R.C. Cammarata, R.K. Eby, J. Mater. Res. 5 (1991) 888.
[24] S. Veprek, S. Reiprich, Thin Solid Films 268 (1996) 64.
[25] F. Vaz, L. Rebouta, P. Godeeau, P. Pacaud, H. Garem, J.P. Riviere, A. Cavaleiro, E. Alves, Surf. Coat. Technol. 133–134 (2000) 307.
[26] C. Louro, A. Cavaleiro, Surf. Coat. Technol. 116–119 (1999) 74.
[27] P.B. Barna, M. Adamik, J. Lábár, L. Köver, J. Tóth, A. Dévényi, R. Manaila, Surf. Coat. Technol. 125 (2000) 147.
[28] J. Musil, Surf. Coat. Technol. 125 (2000) 322.
[29] A.A. Voevodin, J.S. Zabinski, Thin Solid Films 370 (2000) 223.
[30] Th.G. Menzel, K. Bartsch, K. Wetzig, Surf. Coat. Technol. 124 (2000) 190.
[31] F. Vaz, L. Rebouta, S. Carvalho, L.A. Rocha, D. Soares, E. Alves Mater. Sci. Forum (2001) in press.
[32] H. Gleiter, Mechanical properties and deformation behaviour of materials having ultra-fine microstructures, in: M. Nastasi, D.M. Parkin, H. Gleiter (Eds.), Nato ASI Series, 233, Kluwer Academic Publ, Dordrecht, 1993, p. 3.